

# Diversities in the properties of neutron stars at a fixed neutron-skin thickness in $^{208}\text{Pb}$ nucleus

N. Alam<sup>1</sup>, A. Sulaksono<sup>2</sup>, and B. K. Agrawal<sup>1\*</sup>

<sup>1</sup> *Saha Institute of Nuclear Physics, 1/AF Bidhannagar, Kolkata 700064, India*

<sup>2</sup> *Departemen Fisika, FMIPA, Universitas Indonesia, Depok, 16424, Indonesia.*

We study the diversities in the properties of the neutron stars arising due to the different choices for the cross-coupling between various mesons which governs the density dependence of the nuclear symmetry energy in the extended relativistic mean-field(RMF) model. For this purpose, we obtain two different families of the extended RMF model corresponding to different non-linear cross-coupling term in the isovector part of the effective Lagrangian density. The lowest order contributions for the  $\delta$  mesons are also included. The different models within the same family are so obtained that they yield wide variation in the value of neutron-skin thickness in the  $^{208}\text{Pb}$  nucleus. These models are employed to compute the neutron star properties such as, core-crust transition density, radius and red shift at canonical mass ( $1.4M_\odot$ ), tidal polarizability parameter, and threshold mass required for the enhanced cooling through direct Urca process. Most of the neutron star properties considered are significantly different(10%-40%) for the different families of models at a smaller neutron-skin thickness ( $\sim 0.15$  fm) in the  $^{208}\text{Pb}$  nucleus.

PACS numbers: 21.65.Cd, 21.65.Mn, 21.65.Ef, 26.60.Kp

Keywords:

## I. INTRODUCTION

The neutron stars are believed to be composed of highly asymmetric matter, predominantly, the neutrons. Of course, a small admixture of protons, electrons and muons are also present to maintain the  $\beta$ -equilibrium and charge neutrality. The various theoretical models have conjectured the possibility of existence of exotica, like, hyperons, Bose condensates and quarks in the core of the neutron stars [1–8]. The precise knowledge of the masses and the radii of the neutron stars are crucial in determining their compositions. Recently, significant progress has been made along this direction [9]. The masses of PSR J1614-2230 [10] and PSR J0348+0432 [11] are measured to be  $1.97 \pm 0.04M_\odot$  and  $2.01 \pm 0.04M_\odot$ , respectively. These measurements impose the lower bounds on the maximum mass of the neutron stars that a theoretical model must yield. In the absence of the exotic degrees of freedoms, the criterion of maximum mass to be  $\sim 2M_\odot$  is readily satisfied by the theoretical models. The observational constraints on the maximum mass of neutron stars do not completely rule out the possibility of existence of the exotic degrees of freedom, but, the threshold transition densities for their appearance are pushed to 2.5-3.5 times the nuclear saturation density[12–14]. The radii of neutron stars are known only poorly. The values of radii are quite sensitive to the assumed composition of the atmosphere. The radius  $R_{1.4} = 10.7 - 13.1\text{km}$ , for the neutron star with the canonical mass of  $1.4M_\odot$ , is found to be consistent with the observational analysis and the host of experimental data for finite nuclei [15].

The equations of state (EOSs) for the  $\beta$ -equilibrated baryonic matter, employed to determine the bulk properties of neutron stars, are usually constructed using the energy density functionals derived from the Skyrme type effective forces or from an effective Lagrangian density associated with the relativistic mean field (RMF) model. Often, the energy density functionals are optimized using some selected experimental data on a key properties of the finite nuclei. Occasionally, pseudo-data on nuclear and neutron matter are also used in the optimization protocols [16–18]. The EOS for the nuclear matter at a given density and the asymmetry can be viewed for simplicity as,

$$\epsilon(\rho, I) = \epsilon(\rho, 0) + S(\rho)I^2 \quad (1)$$

where,  $\epsilon(\rho, I)$  is the energy per nucleon,  $\rho = \rho_n + \rho_p$ ,  $I = (\rho_n - \rho_p)/\rho$  is the asymmetry with  $\rho_n$  and  $\rho_p$  being densities for the neutrons and the protons. The  $\epsilon(\rho, 0)$  is the EOS for the symmetric nuclear matter and  $S(\rho)$  is the symmetry energy coefficient at a density  $\rho$ . The EOS of the symmetric nuclear matter for the densities up to 4.5 times saturation density ( $\rho_0 = 0.16 \text{ fm}^{-3}$ ) is derived within the reasonable limits by combining the experimental data for the finite nuclei with the collective flow and kaon production data in heavy-ion collisions [19–21]. The poorly known density dependence of  $S(\rho)$  is the major source for uncertainty in the EOS for the asymmetric matter. The value of  $S(\rho)$  is reasonably constrained only around the saturation density by the bulk properties of the finite nuclei. The understanding of density dependence of the  $S(\rho)$  is crucial as it controls the radii of neutron stars, the thicknesses of their crusts, the rate of cooling of neutron stars, and the properties of nuclei involved in r-process nucleosynthesis. The density dependence of the symmetry energy around the saturation den-

---

\*Electronic address: bijay.agrawal@saha.ac.in

sity appears to be well correlated with the neutron-skin thickness  $\Delta r_{\text{np}}$  in a heavy nucleus which can be experimentally measured. The  $\Delta r_{\text{np}}$  is the difference between the rms radii for density distributions of the neutrons and protons in a nucleus. Recently [22, 23], the correlations of the neutron-skin thickness in  $^{208}\text{Pb}$  nucleus with several bulk properties of neutron stars have been examined for the TOV-min and FSU type models. The energy density functional for the TOV-min corresponds to the Skyrme type effective force and that for FSU is based on the extended RMF model. The correlation between neutron-skin thickness in  $^{208}\text{Pb}$  nucleus and the neutron star radius  $R_{1.4}$  for TOV-min is noticeably smaller than the one obtained for the FSU model. Consequently, for the case of TOV-min the properties of neutron stars can have larger variations at a fixed neutron-skin in  $^{208}\text{Pb}$  nucleus. This result is in concordance with the large uncertainties in the high density behaviour of the symmetry energy for the Skyrme type energy density functionals [24].

The tighter correlations of neutron-skin thickness in  $^{208}\text{Pb}$  nucleus with the several properties of the neutron stars within the RMF models seem to be stemming from the lack of freedom in the isovector part of the effective Lagrangian density associated with these models. Most of the RMF models describe the density dependence of the symmetry energy either in terms of the coupling of the isovector-vector  $\rho$  mesons with the nucleons [25] or by including only an additional cross-coupling of isoscalar-scalar  $\sigma$  or isoscalar-vector  $\omega$  with the isovector-vector  $\rho$  mesons [26, 27]. The  $\sigma - \rho$  or  $\omega - \rho$  cross-coupling allows one to vary the neutron-skin thickness over a wide range without significantly affecting the quality of fit to the bulk properties of the nuclei such as the total binding energy and the charge radii [28]. The differences in the high density behaviour of the symmetry energy and their consequences on the properties of the neutron stars arising due to the use of different cross-couplings have never been studied in detail. Further, the inclusion of isovector-scalar  $\delta$  mesons can modify the behaviour of the symmetry energy at high densities [29–31]. In principal, the contributions from the various cross-couplings and the  $\delta$  mesons should be included in a single RMF model. It has not been done so far due to lack of accurate experimental data on the finite nuclei and the neutron stars which govern the isovector part of the RMF model. A comprehensive study of variations in the properties of the neutron stars as a function of the neutron-skin thickness within the RMF models corresponding to different choices for the cross-coupling terms with and without the inclusion of the  $\delta$  mesons may be highly desirable. Such investigation would enable one to understand to what extent the inclusion of contributions from these various cross-couplings and the  $\delta$  mesons within a single RMF model are necessary to describe simultaneously the neutron-skin thickness in  $^{208}\text{Pb}$  and the various neutron star properties.

In the present work, we would like to study the diver-

sities in the properties of the neutron stars arising purely due to the uncertainties in the isovector part of the effective Lagrangian density which governs the density dependence of the nuclear symmetry energy in the extended RMF model. Towards this purpose, two different families of extended RMF models are obtained which mainly differ from each other in the choice for the cross-coupling term in the isovector part of the effective Lagrangian density. One of the families of models includes  $\sigma - \rho$  cross-coupling while the other includes  $\omega - \rho$  cross-coupling term in addition to the various linear and non-linear interaction terms already present in the commonly used RMF models. The contributions due the coupling of the  $\delta$  mesons to the nucleons are also considered. The various coupling constants are so varied that they produce wide variations in the neutron-skin thickness in  $^{208}\text{Pb}$  nucleus without affecting significantly the binding energies and charge radii of the finite nuclei. The various neutron star properties considered are the core-crust transition density, radius for the neutron stars with canonical mass, the tidal polarizability parameter and the threshold mass required for the enhanced cooling through direct Urca process. Some of these neutron stars properties at a fixed neutron-skin thickness differ significantly for two different families of the models.

The paper is organized as follows. In Sec. II, we briefly outline the form of the effective Lagrangian density for the extended RMF model. The procedure adopted to obtain different parameterizations for two different families of the model are described in Sec. III. We also present in this section the results depicting the relationship between different coupling constants which govern the isovector part of the effective Lagrangian density. In Sec. IV, the various properties of the neutron stars obtained for the different families of models are compared for fixed values of neutron-skin thickness in  $^{208}\text{Pb}$  nucleus. The main conclusions are presented in Sec. V.

## II. THEORETICAL FRAME WORK

In the RMF models, nucleons interact through the exchange of isoscalar scalar  $\sigma$ , isoscalar vector  $\omega$  and isovector vector  $\rho$  mesons. The effective Lagrangian density for the RMF model usually includes the cubic and quartic order non-linear self-interaction terms for the  $\sigma$  mesons in addition to the linear terms for the  $\sigma$ ,  $\omega$  and  $\rho$  mesons which describe their interactions with the nucleons. The non-linear self-interaction terms for the  $\sigma$  mesons are added to yield reasonable values for the empirical properties of symmetric nuclear matter. Further, the RMF models are extended by including various cross-couplings terms for these mesons and self-interaction terms for the  $\omega$  and  $\rho$  mesons. The  $\sigma - \rho$  and  $\omega - \rho$  cross-coupling terms enables one to vary the density dependence of the symmetry energy coefficient and the neutron skin thickness in heavy nuclei over a wide range without affecting the other properties of finite nuclei [32, 33]. Most of the

RMF models do not include the contributions from the isovector-scalar  $\delta$  mesons. The bulk properties of the finite nuclei like binding energies and radii are not very sensitive to the presence of the  $\delta$  mesons. However, earlier investigations have stressed the need to include the contributions from the  $\delta$  mesons for proper description of the highly asymmetric dense matter. [29, 31, 34–36].

The effective Lagrangian density which includes the lowest order contribution from the  $\delta$  mesons together with the various non-linear cross-coupling and self-interaction contributions already present in the extended RMF model, can be written as, [29, 35, 37–39],

$$\mathcal{L} = \mathcal{L}_{\mathcal{NM}} + \mathcal{L}_\sigma + \mathcal{L}_\omega + \mathcal{L}_\rho + \mathcal{L}_\delta + \mathcal{L}_{\sigma\omega\rho}, \quad (2)$$

where the Lagrangian  $\mathcal{L}_{\mathcal{NM}}$  describing the interactions of the nucleons through the mesons is,

$$\begin{aligned} \mathcal{L}_{\mathcal{NM}} = & \sum_{J=n,p} \bar{\Psi}_J [i\gamma^\mu \partial_\mu - (M - g_\sigma \sigma - g_\delta \delta \tau)] \Psi_J \\ & - (g_\omega \gamma^\mu \omega_\mu + \frac{1}{2} g_\rho \gamma^\mu \tau \cdot \rho_\mu) \Psi_J. \end{aligned} \quad (3)$$

Here, the sum is taken over the neutrons and protons and  $\tau$  are the isospin matrices. The Lagrangian density  $\mathcal{L}_i$  for  $i = \sigma, \omega, \rho$  and  $\delta$  can be written as,

$$\mathcal{L}_\sigma = \frac{1}{2} (\partial_\mu \sigma \partial^\mu \sigma - m_\sigma^2 \sigma^2) - \frac{\kappa_3}{6M} g_\sigma m_\sigma^2 \sigma^3 - \frac{\kappa_4}{24M^2} g_\sigma^2 m_\sigma^2 \sigma^4, \quad (4)$$

$$\mathcal{L}_\omega = -\frac{1}{4} \omega_{\mu\nu} \omega^{\mu\nu} + \frac{1}{2} m_\omega^2 \omega_\mu \omega^\mu + \frac{1}{24} \zeta_0 g_\omega^2 (\omega_\mu \omega^\mu)^2, \quad (5)$$

$$\mathcal{L}_\rho = -\frac{1}{4} \rho_{\mu\nu} \rho^{\mu\nu} + \frac{1}{2} m_\rho^2 \rho_\mu \rho^\mu, \quad (6)$$

$$\mathcal{L}_\delta = \frac{1}{2} (\partial_\mu \delta \partial^\mu \delta - m_\delta^2 \delta^2). \quad (7)$$

The  $\omega^{\mu\nu}$ ,  $\rho^{\mu\nu}$  are field tensors corresponding to the  $\omega$  and  $\rho$  mesons, and can be defined as  $\omega^{\mu\nu} = \partial^\mu \omega^\nu - \partial^\nu \omega^\mu$  and  $\rho^{\mu\nu} = \partial^\mu \rho^\nu - \partial^\nu \rho^\mu$ . The cross interactions of  $\sigma, \omega$ , and  $\rho$  mesons are described by  $\mathcal{L}_{\sigma\omega\rho}$  which can be written as,

$$\begin{aligned} \mathcal{L}_{\sigma\omega\rho} = & \frac{\eta_1}{2M} g_\sigma m_\omega^2 \sigma \omega_\mu \omega^\mu + \frac{\eta_2}{4M^2} g_\sigma^2 m_\omega^2 \sigma^2 \omega_\mu \omega^\mu \\ & + \frac{\eta_\rho}{2M} g_\sigma m_\rho^2 \sigma \rho_\mu \rho^\mu + \frac{\eta_{1\rho}}{4M^2} g_\sigma^2 m_\rho^2 \sigma^2 \rho_\mu \rho^\mu \\ & + \frac{\eta_{2\rho}}{4M^2} g_\omega^2 m_\rho^2 \omega_\mu \omega^\mu \rho_\mu \rho^\mu. \end{aligned} \quad (8)$$

One also needs to include the contributions from the electromagnetic interaction in the case of finite nuclei. The Lagrangian density  $\mathcal{L}_{em}$  for the electromagnetic interaction can be written as,

$$\mathcal{L}_{em} = -\frac{1}{4} F_{\mu\nu} F^{\mu\nu} - e \bar{\Psi}_p \gamma_\mu A_\mu \Psi_p, \quad (9)$$

where,  $A$  is the photon field and  $F^{\mu\nu} = \partial^\mu A^\nu - \partial^\nu A^\mu$ . The equation of motion for nucleons, mesons and photons can be derived from the Lagrangian density defined in Eq.(2). The contributions from Eq. (9) are included only for the case of finite nuclei.

It is clear from (8) that there are five cross-coupling terms; two of them are the cubic order terms corresponding to the  $\sigma - \omega$  and  $\sigma - \rho$  cross-couplings and the remaining are the quartic order terms. The contribution from the  $\sigma - \omega$  cross-couplings and self coupling of  $\omega$  mesons play important role in varying the high density behaviour of the EOSs and also prevents instabilities in them [26, 40, 41]. The contributions of the self-coupling of  $\rho$  mesons are not considered in Eq. (6), since, expectation value of the  $\rho$  meson field is order of magnitude smaller than that for the  $\omega$  meson field [38]. The inclusion of the  $\rho$  meson self interaction can affect the properties of the finite nuclei and neutron stars only very marginally [41]. Of the particular interest in the present work are the cross-coupling terms involving  $\rho$  meson field which contributes to the isovector part of the effective Lagrangian density in addition to the usual linear couplings of the  $\rho$  and  $\delta$  mesons to the nucleons. We shall mainly focus on the lowest order  $\sigma - \rho$  and  $\omega - \rho$  cross-couplings whose strengths are determined by the values of  $\eta_\rho$  and  $\eta_{2\rho}$ . The quartic order  $\sigma - \rho$  cross-coupling strength  $\eta_{1\rho}$  is set to zero. The values of  $\eta_\rho$  or  $\eta_{2\rho}$  can be appropriately adjusted to yield wide variations in the density dependence of the symmetry energy coefficient and the neutron skin thickness in heavy nuclei without affecting the other properties of finite nuclei [32, 33, 42].

### III. MODEL PARAMETERS

Two different families of the extended RMF models, named hereafter as  $F_\rho$  and  $F_{2\rho}$ , are obtained. These families differ from each other in the choice for the cross-coupling term in the isovector part of the Lagrangian density. The isovector part of the Lagrangian density for the  $F_\rho(F_{2\rho})$  family is governed by the coupling parameters  $g_\rho$ ,  $g_\delta$  and  $\eta_\rho(\eta_{2\rho})$ . The parameters  $g_\rho$  and  $g_\delta$  denote the strengths for the coupling of the  $\rho$  and  $\delta$  mesons to the nucleons, respectively. The parameter  $\eta_\rho$  and  $\eta_{2\rho}$  denote the strength of the  $\sigma - \rho$  and  $\omega - \rho$  cross-couplings as can be seen from Eq. 8. The remaining parameters which correspond to the isoscalar part of the Lagrangian density and the mass of the  $\sigma$ ,  $\omega$  and  $\rho$  mesons are kept fixed to that of the BKA22 model [43]. The BKA22 model has been identified to satisfy various constraints related to symmetric nuclear matter, pure neutron matter, symmetry energy, and its derivatives [44].

The different parameterizations of  $F_\rho(F_{2\rho})$  families are obtained by varying appropriately the values of  $g_\rho$ ,  $g_\delta$  and  $\eta_\rho(\eta_{2\rho})$ . For a given value of  $g_\delta$  and  $\eta_\rho(\eta_{2\rho})$ , the value of  $g_\rho$  is always adjusted to yield appropriate binding energy for the  $^{208}\text{Pb}$  nucleus. Once the values of  $g_\delta$ ,  $g_\rho$  and  $\eta_\rho$  or  $\eta_{2\rho}$  are known, the properties of the nuclear matter and

TABLE I: The parameters of the isovector part of the Lagrangian density for some representative sets for the  $F_\rho$  and  $F_{2\rho}$  families of models. In the bottom part, the values for the symmetry energy coefficient at the saturation density  $J$ , symmetry energy slope parameter  $L$ , effective mass for the protons and neutrons and their differences are also presented. All these quantities are in MeV.

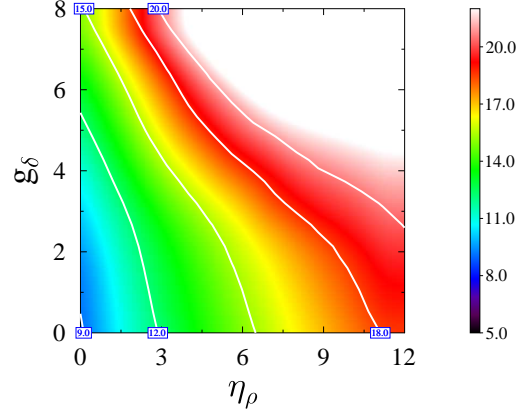
| Parameter         | $F_\rho$ |        | $F_{2\rho}$ |        |
|-------------------|----------|--------|-------------|--------|
|                   | SET1     | SET2   | SET3        | SET4   |
| $\eta_\rho$       | 4.0      | 4.0    | 0.0         | 0.0    |
| $\eta_{2\rho}$    | 0.0      | 0.0    | 17.5        | 17.5   |
| $g_\delta$        | 0.0      | 8.0    | 0.0         | 8.0    |
| $g_\rho$          | 13.033   | 21.863 | 11.051      | 18.556 |
| $J$               | 33.3     | 30.9   | 33.0        | 30.2   |
| $L$               | 79.0     | 62.5   | 65.0        | 23.3   |
| $M_p^*$           | 570.1    | 630.9  | 577.8       | 652.4  |
| $M_n^*$           | 570.1    | 495.4  | 577.8       | 515.8  |
| $\Delta M_{pn}^*$ | 0.0      | 135.5  | 0.0         | 136.6  |

TABLE II: The values of the total binding energy ( $E$ ) in MeV, charge radii ( $r_c$ ), neutron radii ( $r_n$ ) and neutron-skin thickness  $\Delta r_{np}$  in fm for a few asymmetric spherical nuclei obtained for SET1 - SET4 parameters.

| Nucleus           | Property        | $F_\rho$ |          | $F_{2\rho}$ |          |
|-------------------|-----------------|----------|----------|-------------|----------|
|                   |                 | SET1     | SET2     | SET3        | SET4     |
| $^{48}\text{Ca}$  | $E$             | -415.75  | -415.40  | -415.81     | -415.61  |
|                   | $r_c$           | 3.468    | 3.484    | 3.465       | 3.477    |
|                   | $r_n$           | 3.575    | 3.544    | 3.574       | 3.535    |
|                   | $\Delta r_{np}$ | 0.201    | 0.153    | 0.202       | 0.151    |
| $^{132}\text{Sn}$ | $E$             | -1102.49 | -1100.37 | -1102.69    | -1100.99 |
|                   | $r_c$           | 4.736    | 4.759    | 4.727       | 4.731    |
|                   | $r_n$           | 4.952    | 4.901    | 4.934       | 4.873    |
|                   | $\Delta r_{np}$ | 0.284    | 0.210    | 0.286       | 0.210    |
| $^{208}\text{Pb}$ | $E$             | -1637.07 | -1637.08 | -1637.06    | -1637.05 |
|                   | $r_c$           | 5.545    | 5.566    | 5.535       | 5.538    |
|                   | $r_n$           | 5.706    | 5.659    | 5.699       | 5.631    |
|                   | $\Delta r_{np}$ | 0.219    | 0.151    | 0.221       | 0.151    |

the finite nuclei can be computed. We vary the values of  $g_\delta$  over a wide range from 0 to 8. The values of  $\eta_\rho$  and  $\eta_{2\rho}$  are varied in the range of 0 – 12 and 0 – 60, respectively. For  $\eta_\rho > 12$ , the stable solutions of the field equations for the mesons could not be obtained. We have constructed 22 different parameterizations of the  $F_\rho$  and 41 different parameterizations of the  $F_{2\rho}$  families.

The Fig. 1 displays the relationship between the various parameters of the isovector channel for the  $F_\rho$  and  $F_{2\rho}$  families of the models. It can be readily seen that the value of  $g_\rho$ , required to reproduce the binding energy for the  $^{208}\text{Pb}$  nucleus, increases with  $g_\delta$ ,  $\eta_\rho$  and  $\eta_{2\rho}$ . In other words, the equation of state at least for the densities relevant for the finite nuclei becomes softer with the increase in the  $g_\delta$ ,  $\eta_\rho$  and  $\eta_{2\rho}$ , which is compensated by increasing the value of  $g_\rho$  to reproduce the binding energy for the  $^{208}\text{Pb}$  nucleus. In the Fig. 2, the relationship of the parameters  $g_\delta$  and  $\eta_\rho(\eta_{2\rho})$  with the symmetry energy coefficient at the saturation density ( $J = S(\rho_0)$ ) for the  $F_\rho(F_{2\rho})$  is displayed in terms of the contour plots.



$g_\rho$  ALONG THE CONTOUR LINES

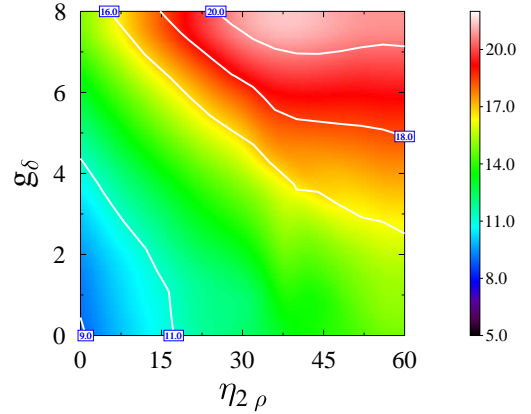
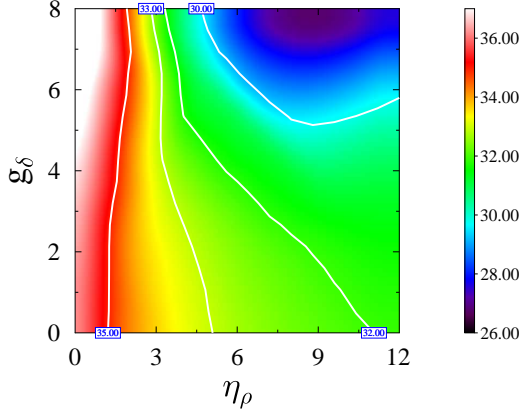


FIG. 1: (Color online) Colour coded contours in the  $g_\delta - \eta_\rho$  (upper panel) and  $g_\delta - \eta_{2\rho}$  (lower panel) planes corresponding to the  $F_\rho$  and  $F_{2\rho}$  families, respectively. The value of  $g_\rho$  are colour coded according to the scale one the right side.

Similarly, the results for the  $\Delta r_{np}$  in the  $^{208}\text{Pb}$  nucleus are plotted in Fig. 3. In general, the values of  $J$  and  $\Delta r_{np}$  decreases with increasing  $g_\delta$ ,  $\eta_\rho$  or  $\eta_{2\rho}$ . The  $F_{2\rho}$  model yields larger variations in  $\Delta r_{np}$ . The large values for  $\eta_\rho$  are not favored, as a result the  $F_\rho$  family can yield very small values of  $\Delta r_{np}$  only with the inclusion of the  $\delta$  mesons. In Table I the values of the parameters for four representative sets corresponding to the  $F_\rho$  and  $F_{2\rho}$  models are listed. The SET1 and SET2 belong to the  $F_\rho$  family, while, SET3 and SET4 are for the  $F_{2\rho}$  family. The SET1 and SET3 do not include the contributions from the  $\delta$  mesons ( $g_\delta = 0$ ). The SET2 and SET4 correspond to the highest value of the  $\delta$ -nucleon coupling strength ( $g_\delta = 8$ ), otherwise, they are very much similar to the SET1 and SET3, respectively. These different sets are so chosen that the comparison of the properties of the neutron stars resulting from them would give us





J ALONG THE CONTOUR LINES

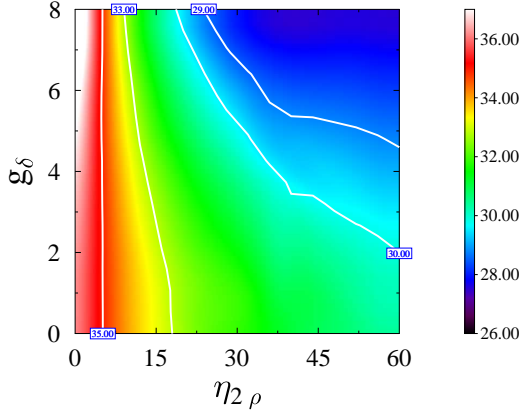


FIG. 2: (Color online) Same as Fig. 1, but, for the symmetry energy at the saturation density ( $J = S(\rho_0)$ ) fixed along the contour. The values of  $J$  are in MeV.

a crude estimate about the effects of  $\delta$  meson as well as the  $\sigma - \rho$  and  $\omega - \rho$  cross-couplings. In the bottom part of Table I, the values of the symmetry energy coefficient at the saturation density ( $J = S(\rho_0)$ ), symmetry energy slope parameter ( $L = \left(3\rho \frac{\partial S(\rho)}{\partial \rho}\right)_{\rho_0}$ ), proton and neutron effective masses and their differences are also presented. The effective masses are obtained at the maximum asymmetry, i.e., the pure neutron matter. In Table II, we present some bulk properties of a few asymmetric spherical nuclei. The various bulk properties for these nuclei are relatively better reproduced for the SET1 and SET3 parameters which corresponds to  $\Delta r_{\text{np}} \sim 0.22 \text{ fm}$  in the  $^{208}\text{Pb}$  nucleus, since, this value of  $\Delta r_{\text{np}}$  is almost the same as that of the base model BKA22. It may be noted that the  $\Delta r_{\text{np}} = 0.22 \text{ fm}$  for the SET1 and SET3, but, they belong to different families. Similarly, SET2 and SET4 represent different families, with  $\Delta r_{\text{np}} = 0.15 \text{ fm}$ .

Let us now take a look at the density dependence of

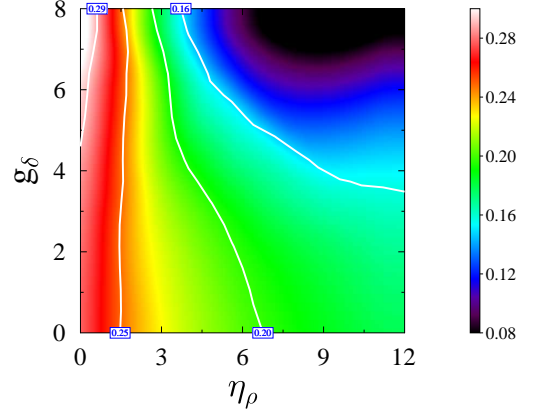
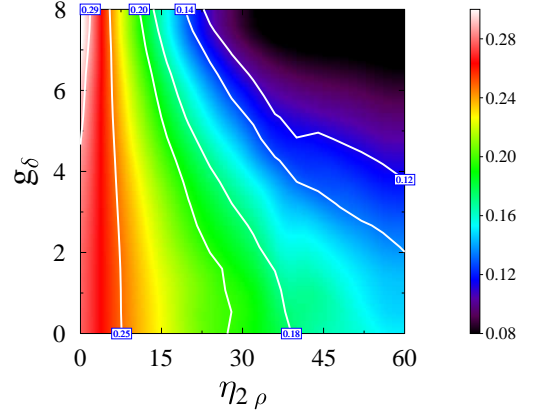
 $\Delta r_{\text{np}}$  ALONG THE CONTOUR LINES

FIG. 3: (Color online) Same as Fig. 1, but, for the neutron skin thickness  $\Delta r_{\text{np}}$  in the  $^{208}\text{Pb}$  nucleus fixed along the contour. The values of  $\Delta r_{\text{np}}$  are in fm.

the symmetry energy for the different parameterizations of the  $F_\rho$  and  $F_{2\rho}$  families corresponding to equal values of  $\Delta r_{\text{np}}$ . In Fig. 4, we display the variations of symmetry energy as a function of density for different parameterizations as indicated by SET1, SET2, SET3 and SET4. The high density behaviour for the symmetry energy is stiffer for the  $F_\rho$  family as can be easily verified by comparing the results for the SET1 and SET2 with those for the SET3 and SET4, respectively. Further, by comparing the results for the SET1 with SET2 or those for SET3 with SET4, it can be concluded that the inclusion of the  $\delta$  mesons softens the symmetry energy at low densities while makes it stiffer at higher densities. The results depicted in Fig. 4 provide evidences a priori about the possibilities of the differences in the properties of neutron stars at a fixed  $\Delta r_{\text{np}}$  across the different families of the models, due to the differences in the high density behaviour of the symmetry energy.

#### IV. NEUTRON-SKIN THICKNESS AND PROPERTIES OF NEUTRON STARS

We wish to study the differences in the properties of neutron stars for the  $F_\rho$  and  $F_{2\rho}$  families of the models at fixed values for the neutron skin thickness  $\Delta r_{\text{np}}$  in the  $^{208}\text{Pb}$  nucleus. In particular, attention is given to the study of such differences at  $\Delta r_{\text{np}} = 0.15\text{fm}$  in  $^{208}\text{Pb}$  nucleus. This value of  $\Delta r_{\text{np}}$  is consistent with  $0.156^{+0.025}_{-0.021}\text{fm}$  [45] and  $0.168 \pm 0.022\text{fm}$  [46] as extracted from the experimental data on the dipole polarizability for  $^{208}\text{Pb}$  nucleus. A very recent measurement of coherent pion photo-production [47] also corresponds to  $\Delta r_{\text{np}} = 0.15 \pm 0.03\text{fm}$  in  $^{208}\text{Pb}$  nucleus. However, these measurements do not conclusively yet rule out the larger values for  $\Delta r_{\text{np}}$ , since, the Lead Radius Experiment (PREX) [28, 48, 49] has recently measured  $\Delta r_{\text{np}} = 0.33^{+0.16}_{-0.18}\text{fm}$  in  $^{208}\text{Pb}$  nucleus via parity-violating electron scattering which provides the first purely electroweak, almost model independent estimate. Our purpose is to give quantitative estimates about the extent to which the various properties of the neutron stars might vary across the different families of the models for a plausible value of neutron-skin thickness. The various properties for the neutron stars considered are the core-crust transition density, radius, red-shift, the threshold mass required for the enhance cooling through the direct Urca process and the tidal polarizability parameter. The comparison of results for the  $F_\rho$  and  $F_{2\rho}$  families of the models would enable us to understand the role of different cross-coupling terms. We shall also assess the effects of the  $\delta$  mesons by comparing the results obtained with and without its inclusion in the same family of the models.

The values of the neutron-skin thickness in a heavy nucleus, according to the Droplet Model [50], are strongly correlated with the symmetry energy slope parameter  $L$ . The dependence of  $L$  on  $\Delta r_{\text{np}}$  in  $^{208}\text{Pb}$  for the  $F_\rho$  and  $F_{2\rho}$  families of the models are displayed in Fig. 5. It may be pointed out that the similar values of  $\Delta r_{\text{np}}$  can be obtained within a given family by varying appropriately the values of coupling parameters  $g_\delta$  and  $\eta_\rho$  or  $\eta_{2\rho}$  (see also Fig. 3). The solid and the hollow symbols represent the results obtained with and without the contributions from the  $\delta$  mesons, respectively. The values of  $\Delta r_{\text{np}}$  are well correlated with  $L$  within a given family of the models irrespective of the contributions from the  $\delta$  mesons. However, the values of  $L$  for the two families of the models differ significantly at smaller  $\Delta r_{\text{np}}$ . This difference gradually disappears as  $\Delta r_{\text{np}}$  increases.

The values of core-crust transition density  $\rho_t$  and the corresponding pressure  $P_t$  as a function of  $\Delta r_{\text{np}}$  obtained for  $F_\rho$  and  $F_{2\rho}$  families of models are plotted in Fig. 6. The values of  $\rho_t$  are obtained using a method based on the relativistic random-phase approximation [51–54]. This method uses the fact that the uniform matter in its ground state at sufficiently low densities becomes unstable to small density fluctuations. The values of  $\rho_t$  are correlated with the  $\Delta r_{\text{np}}$  within a same family irrespec-

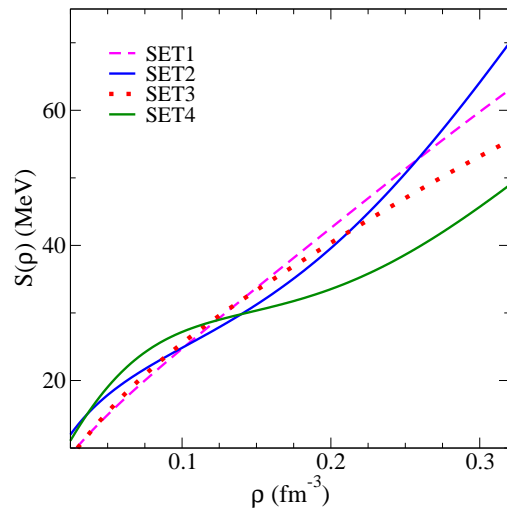


FIG. 4: (Color online) The density dependence of symmetry energy  $S(\rho)$  for some representative cases of  $F_\rho$  and  $F_{2\rho}$  families of the models. The labels SET1 and SET2 correspond to the two different parameterizations for the  $F_\rho$  family, whereas, the SET3 and SET4 correspond to the  $F_{2\rho}$  family. The SET1 and SET3 are associated with  $\Delta r_{\text{np}} = 0.22\text{fm}$  and the SET2 and SET4 yield  $\Delta r_{\text{np}} = 0.15\text{fm}$  (see also Tables I and II).

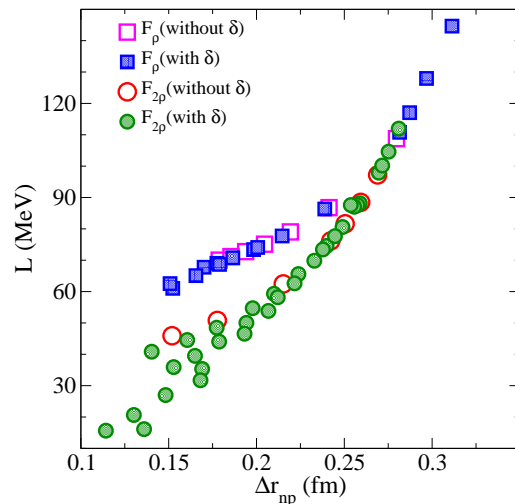


FIG. 5: (Color online) The variations of symmetry energy slope parameter  $L$  with neutron-skin thickness  $\Delta r_{\text{np}}$  in the  $^{208}\text{Pb}$  nucleus for the  $F_\rho$  and  $F_{2\rho}$  families of models. The solid and hollow symbols represent the results obtained with ( $g_\delta \neq 0$ ) and with ( $g_\delta = 0$ ), respectively.

tive of the contributions from the  $\delta$  mesons. But, this correlation seems to be somewhat model dependent—the values of  $\rho_t$  for both the families of models at a fixed  $\Delta r_{\text{np}}$  are not the same. In particular, the  $\rho_t$  is significantly larger for the  $F_{2\rho}$  family at smaller  $\Delta r_{\text{np}}$ . The transition pressure  $P_t$  is not very well correlated with the  $\Delta r_{\text{np}}$ . Initially, the  $P_t$  increases with  $\Delta r_{\text{np}}$  and it

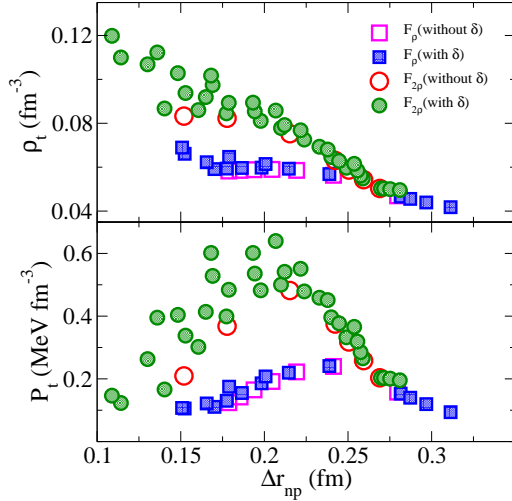


FIG. 6: (Color online) The variation of core-crust transition density and the corresponding pressure with the neutron-skin thickness  $\Delta r_{np}$  in  $^{208}\text{Pb}$  nucleus for the  $F_\rho$  and  $F_{2\rho}$  families of the extended RMF models.

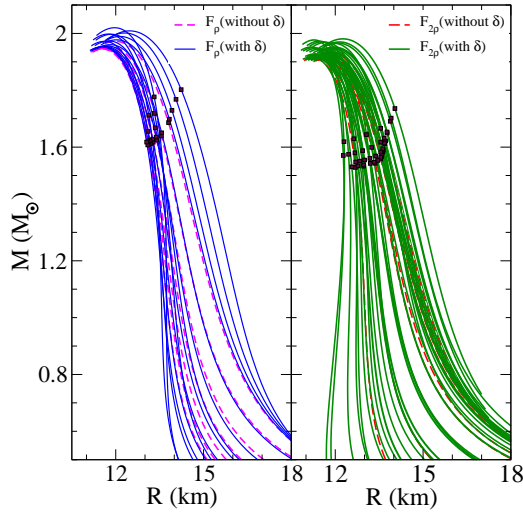


FIG. 7: (Color online) The mass-radius relationship for the  $F_\rho$  and  $F_{2\rho}$  families of the models. The solid squares represent the masses and the corresponding radii for the neutron stars with the central density to be  $3\rho_0$ .

decreases for higher values of  $\Delta r_{np}$ .

Once, the core-crust transition density is determined, the EOS for various density ranges as required for the computation of the properties of the neutron stars can be constructed. The EOS data for the density  $\rho \sim 4.8 \times 10^{-9} - 2.6 \times 10^{-4} \text{ fm}^{-3}$  corresponding to the outer crust region are taken from Ref. [55]. The EOS for the inner crust is obtained by assuming a polytropic form  $P(\epsilon) = a + b\epsilon^{4/3}$ , where  $P$  and  $\epsilon$  are the pressure and energy density respectively. The constants  $a$  and  $b$  are determined in such a way that the EOS for the inner crust matches with that for the inner edge of the outer crust

at one end and with the edge of the core at the other end. The EOSs for the core region,  $\rho > \rho_t$ , are obtained within the RMF model by using the different parameterizations of the  $F_\rho$  and  $F_{2\rho}$  families. The core region is assumed to be composed of neutrons, protons, electrons and muons. The chemical potentials for various particle species at a given baryon density are obtained by imposing the  $\beta$ -equilibrium and charge neutrality conditions. We use these EOSs to compute the properties of static neutron stars by integrating the Tolman-Oppenheimer-Volkoff (TOV) equations [56]. In Fig. 7 we display the mass-radius relationship for the sequences of static neutron stars obtained for the  $F_\rho$  and  $F_{2\rho}$  families of models. The solid and the dashed lines depict the results obtained with and without the inclusion of the contributions from the  $\delta$  mesons, respectively. The solid squares represent the masses and the corresponding radii for the neutron stars with the central density to be  $3\rho_0$ . The different EOSs obtained for a given family of the models differ mainly in the high density behaviour of the symmetry energy. This leads to the variations in the mass-radius relationship for the neutron stars within the same family of the models. The maximum mass  $M_{\text{max}} = 1.95 - 2.02 M_\odot$  and  $1.91 - 1.98 M_\odot$  and the radii  $R_{1.4} = 13.3 - 15.4 \text{ km}$  and  $12.3 - 14.9 \text{ km}$  for the  $F_\rho$  and  $F_{2\rho}$  families, respectively. The value of  $M_{\text{max}}$  for the  $F_\rho$  family is consistent with the recent mass measurements  $M = 1.97 \pm 0.04 M_\odot$  for PSR J1614-2230 [10] and  $M = 2.01 \pm 0.04 M_\odot$  for PSR J0348+0432 [11], but, the values for  $R_{1.4}$  is marginally away from the  $R_{1.4} = 10.7 - 13.1 \text{ km}$  as extracted in Ref. [15]. For the  $F_{2\rho}$  family, values for  $M_{\text{max}}$  are barely consistent with the recent measurements, but,  $R_{1.4}$  is consistent with the ones extracted in Ref. [15]. The inclusion of the  $\delta$  mesons yields higher values for the maximum mass for the neutron stars within a family. A more realistic estimation for the effects of  $\delta$  mesons on the maximum mass of the neutron stars requires the inclusion of various exotic degrees of freedom. Since, the density at the center of the neutron star with the maximum mass for our EOSs is significantly larger than  $3\rho_0$ .

We now compare the various properties of the neutron stars at fixed values of  $\Delta r_{np}$  obtained for the  $F_\rho$  and  $F_{2\rho}$  families. Before embarking on our discussion, it may be reminded that the dependence of the various neutron star properties on the neutron-skin thickness are merely due to the fact that different models differ only in the density dependence of the symmetry energy. The EOS for the symmetric nuclear matter is taken to be the same for all the models, since, our goal is to study the diversities in the properties of the neutron stars arising purely due to the differences in the density dependence of the symmetry energy within the extended RMF model. In Fig. 8 the radii and red shifts for the neutron stars with mass  $1.4 M_\odot$  are plotted against the  $\Delta r_{np}$ . The spread in  $R_{1.4}$  and  $Z_{1.4}$  for several cases corresponding to the similar  $\Delta r_{np}$  within the same family is smaller. The values of  $R_{1.4}$  and  $Z_{1.4}$  obtained for two different families differ noticeably at the smaller values of  $\Delta r_{np}$ . For  $\Delta r_{np} = 0.15$

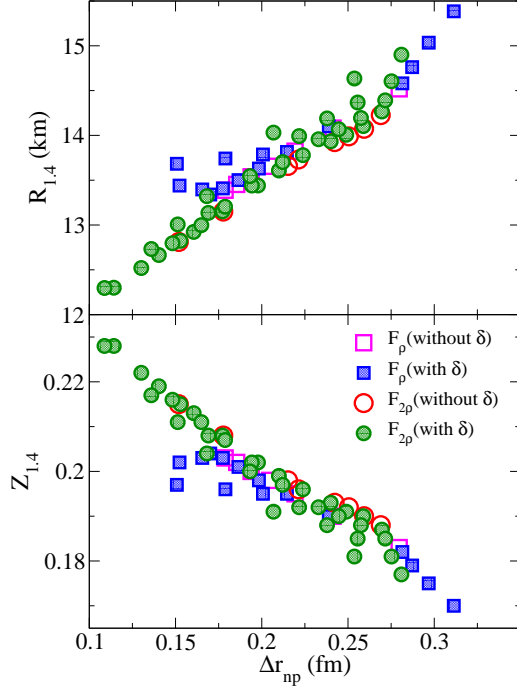


FIG. 8: (Color online) Plots for the radius  $R_{1.4}$  for the neutron stars with the canonical mass  $1.4M_\odot$  (upper panel) and the corresponding red shift (lower panel) as a function of  $\Delta r_{np}$  in the  $^{208}\text{Pb}$  nucleus obtained for the  $F_\rho$  and  $F_{2\rho}$  families of models.

fm the maximum differences in the values of  $R_{1.4}$  and  $Z_{1.4}$  obtained for the two families are  $\sim 1.0$  km and 0.02, respectively. In Fig. 9 We display our results for threshold mass the  $M_{DU}$  required for the enhanced cooling of neutron stars by means of neutrino emission from the nucleons in the direct Urca process [57]. The values of  $M_{DU}$  are quite sensitive to the neutron-skin thickness. The value of  $M_{DU}$  for the  $F_{2\rho}$  family can vary over the range of  $0.8 - 1.9M_\odot$  with  $\Delta r_{np}$  decreasing from 0.3fm to 0.1fm. This variation is little smaller for the case of  $F_\rho$  family. The value of  $M_{DU}$  for both the families differ quite significantly at smaller  $\Delta r_{np}$ . At  $\Delta r_{np} = 0.15$  fm the difference between the values of  $M_{DU}$  for both the families is about  $0.6M_\odot$  which is quite significant (40%).

We now consider our results for the tidal polarizability parameter  $\lambda$  defined as,

$$Q_{ij} = -\lambda \mathcal{E}_{ij}, \quad (10)$$

where,  $Q_{ij}$  is the induced quadrupole moment of a star in binary due to the static external tidal field of the companion star  $\mathcal{E}_{ij}$ . The parameter  $\lambda$  can be expressed in terms of the dimensionless quadrupolar tidal Love number  $k_2$  as,

$$\lambda = \frac{2}{3G} k_2 R^5, \quad (11)$$

where,  $R$  is the radius of a isolated neutron star, i.e., long before merger. The value of  $k_2$  depends on the stel-

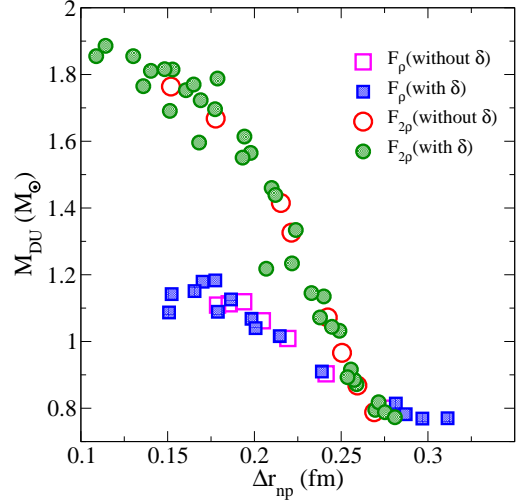


FIG. 9: (Color online) The dependence of the threshold neutron star mass  $M_{DU}$  on the neutron-skin thickness in  $^{208}\text{Pb}$  nucleus. The neutron stars with mass equal to or larger than  $M_{DU}$  undergo enhanced cooling through direct Urca process for the cooling.

lar structure and can be calculated by following the procedure used in Refs. [58–60]. The values of  $\lambda$  for the neutron stars with masses  $\sim 1M_\odot$  are sensitive to the behaviour of the symmetry energy at supra-nuclear densities [61]. In Fig. 10, we plot the values of  $\lambda$  as a function of neutron star mass obtained for different parameterizations for the  $F_\rho$  and  $F_{2\rho}$  families. The value of  $\Delta r_{np}$  is equal to 0.15 fm for all of these cases. The differences in the tidal polarizability at low mass neutron star for the two different families is very small. But the difference increases as the mass increases due to different high density behaviour of the symmetry energy for different families of models. The values of  $\lambda$  for the neutron star with canonical mass vary over a wide range of  $2.7 \times 10^{36}$  to  $4.3 \times 10^{36} \text{ cm}^2 \text{gs}^2$ . The value of  $\lambda$  at  $1.4M_\odot$  obtained for the  $F_\rho$  family is about 1.5 times larger than that for the  $F_{2\rho}$  family. The inclusion of  $\delta$  mesons slightly lowers the value of tidal polarizability of neutron star with mass  $1.4M_\odot$ . On passing, it may be remarked that the differences in  $\lambda$  across the two different families of the models are larger than the uncertainties expected in its measurement by the advanced LIGO-Vergo detector and Einstein Telescope [60, 62].

Finally, we have collected in Table III the results for the various properties of the neutron stars obtained for a few representative cases corresponding to the  $F_\rho$  and  $F_{2\rho}$  families. The values of neutron-skin thickness for the  $^{208}\text{Pb}$  nucleus are also listed. The comparison of the results obtained for the SET1 with those for SET3 or SET2 with SET4 readily gives a crude estimate about the variation in the properties of the neutron stars across the different families of models at a fixed neutron-skin thickness. Similarly, the idea about the effects of  $\delta$  mesons



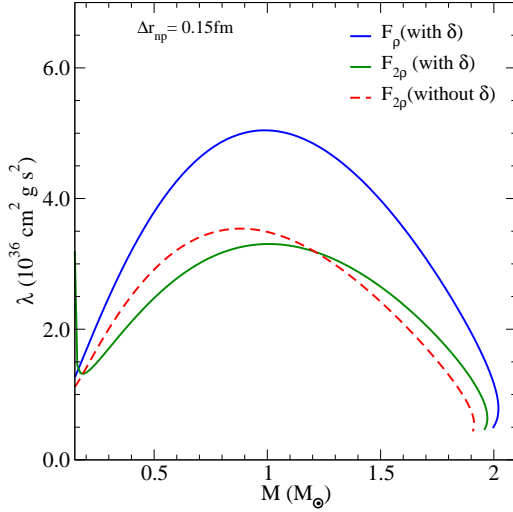


FIG. 10: (Color online) Variations in the tidal polarizability parameter  $\lambda$  with the neutron star mass for the different parameterizations of  $F_\rho$  and  $F_{2\rho}$  families corresponding to neutron-skin thickness  $\Delta r_{np} = 0.15$  fm in the  $^{208}\text{Pb}$  nucleus.

TABLE III: Properties of neutron stars and the neutron-skin thickness in the  $^{208}\text{Pb}$  nucleus obtained for SET1 -SET4 parameters. The values of tidal polarizability parameter  $\lambda_{1.4}$ , listed in the last row, correspond to the neutron star with mass  $1.4M_\odot$ .

| Properties                                     | $F_\rho$ |       | $F_{2\rho}$ |       |
|--|----------|-------|-------------|-------|
|  | SET1     | SET2  | SET3        | SET4  |
| $\Delta r_{np}$ (fm)                           | 0.22     | 0.15  | 0.22        | 0.15  |
| $\rho_{DU}$ (fm) $^{-3}$                       | 0.297    | 0.282 | 0.401       | 0.505 |
| $\rho_t$ (fm) $^{-3}$                          | 0.058    | 0.069 | 0.073       | 0.107 |
| $P_t$ (MeV fm $^{-3}$ )                        | 0.222    | 0.107 | 0.474       | 0.509 |
| $R_{1.4}$ (km)                                 | 13.08    | 12.96 | 13.00       | 12.37 |
| $R_{\text{max}}$ (km)                          | 11.40    | 11.68 | 11.29       | 11.28 |
| $M_{DU}(M_\odot)$                              | 1.01     | 1.09  | 1.33        | 1.69  |
| $\lambda_{1.4}$ ( $10^{36}$ cm $^2$ g s $^2$ ) | 3.41     | 4.33  | 2.87        | 2.88  |

within the same family can be obtained by comparing the results for SET1 with SET2 or SET3 with SET4. It may be easily verified from Table III and Figs. 8 - 10 that the values of core-crust transition density  $\rho_t$ ,  $R_{1.4}$ ,  $M_{DU}$  and the tidal polarizability parameter  $\lambda$  for both the families of the models can differ significantly at a fixed value of  $\Delta r_{np}$ . Thus, instead of the  $\sigma - \rho$  and  $\omega - \rho$  cross-couplings as included separately in the different families of the models, a linear combinations of these cross-couplings in a single model would allow one to adjust the properties of the neutron stars over a wide range at a fixed value of the neutron skin thickness in a heavy nucleus, like,  $^{208}\text{Pb}$ . Furthermore, the presence of  $\delta$  mesons enable ones to obtain the models with smaller value of neutron-skin thickness as can be seen from Fig. 3.

## V. CONCLUSIONS

We have studied the differences in the various properties of the neutron stars arising mainly due to the uncertainties in the density content of the nuclear symmetry energy in the extended RMF model. With this aim, two different families of the extended RMF model, namely,  $F_\rho$  and  $F_{2\rho}$  are obtained. The  $F_\rho$  family includes  $\sigma - \rho$  cross-coupling, while, the  $F_{2\rho}$  family includes  $\omega - \rho$  cross-coupling. Both the families of models include the contributions from the  $\delta$  meson in addition to several linear and non-linear interaction terms already present in the commonly used RMF models. The several parameterizations for each of the families of the models are so obtained that they yield wide variations for the neutron-skin thickness  $\Delta r_{np}$  in the  $^{208}\text{Pb}$  nucleus without affecting much the other bulk properties of the nuclei. The inclusion of  $\delta$  meson produces required splitting in the effective mass for the neutrons and protons and also enables us to obtain smaller neutron-skin thickness.

We compare the various properties of neutron stars obtained for the  $F_\rho$  and  $F_{2\rho}$  families. The properties of neutron stars considered are the core-crust transition density, radius, red shift, tidal polarizability parameter and threshold mass required for the enhanced cooling through direct Urca process. Most of these properties of the neutron stars at a fixed  $\Delta r_{np}$  are noticeably different for two different families of the models. These differences are pronounced at smaller values of  $\Delta r_{np}$  which can be attributed to the differences in the density dependence of the symmetry energy resulting due to different cross-coupling terms. For  $\Delta r_{np} = 0.15$  fm in the  $^{208}\text{Pb}$  nucleus, consistent with the current experimental data on dipole polarizability, the red-shift and the radius of neutron stars with mass  $1.4M_\odot$  differs by about 10% for the two families of models. Such differences are quite significant ( $\sim 40\%$ ) for the tidal polarizability parameter for the neutron stars with mass  $1.4M_\odot$  and the threshold mass required for the direct Urca process to occur in the neutron stars. The values of the core-crust transition density also differs reasonably across the different families of the models. We may thus say that the simultaneous inclusion of the  $\sigma - \rho$  and  $\omega - \rho$  cross-couplings in the extended RMF model would enhance its flexibility to accommodate the variations in the properties of the neutron stars at a given neutron-skin thickness.

## Acknowledgments

A.S. acknowledges the support given by Universitas Indonesia and would like to thank SINP for the hospitality during his visit where this work was initiated. The authors gratefully acknowledge the assistance of Tanuja Agrawal in the preparation of the manuscript.

- 
- [1] N. K. Glendenning and S. A. Moszkowski, Phys. Rev. Lett. **67**, 2414 (1991).
- [2] N. K. Glendenning and J. Schaffner-Bielich, Phys. Rev. Lett. **81**, 4564 (1998).
- [3] B. D. Lackey, M. Nayyar, and B. J. Owen, Phys. Rev. D **73**, 024021 (2006).
- [4] H.-J. Schulze, A. Polls, A. Ramos, and I. Vidaña, Phys. Rev. C **73**, 058801 (2006).
- [5] J. M. Lattimer and M. Prakash, Phys. Rep. **442**, 109 (2007).
- [6] I. Bednarek and R. Manka, Eur. Phys. Lett. **78**, 32001 (2007).
- [7] J. Schaffner-Bielich and A. Gal, Phys. Rev. C **62**, 034311 (2000).
- [8] N. Chamel, P. Haensel, J. L. Zdunik, and A. F. Fantina, Int. J. Mod. Phys. E **22**, 1330018 (2013).
- [9] J. M. Lattimer, Annu. Rev. Nucl. Part. Sci. **62**, 485 (2012).
- [10] P. B. Demorest, T. Pennucci, S. M. Ransom, M. S. E. Roberts, and J. W. T. Hessels, Nature **467**, 1081 (2010).
- [11] J. Antoniadis, P. C. C. Freire, N. Wex, T. M. Tauris, R. S. Lynch, M. H. van Kerkwijk, M. Kramer, C. Bassa, V. S. Dhillon, T. Driebe, et al., Science **340**, 448 (2013).
- [12] D. Lonardonì, A. Lovato, S. Gandolfi, and F. Pederiva, Phys. Rev. Lett. **114**, 092301 (2015).
- [13] Y. Lim, K. Kwak, C. H. Hyun, and C.-H. Lee, Phys. Rev. C **89**, 055804 (2014).
- [14] A. Sulaksono and B. K. Agrawal, Nucl. Phys. **A895**, 44 (2012).
- [15] J. M. Lattimer and Y. Lim, Astrophys. J. **771**, 51 (2013).
- [16] E. Chabanat, P. Bonche, P. Haensel, J. Meyer, and R. Schaeffer, Nucl. Phys. **A627**, 710 (1997).
- [17] B. K. Agrawal, J. N. De, and S. K. Samaddar, Phys. Rev. Lett. **109**, 262501 (2012).
- [18] F. J. Fattoyev, W. Newton, J. Xu, and B.-A. Li, J. Phys. Conf. Ser. **420**, 012108 (2013).
- [19] P. Danielewicz, R. Lacey, and W. G. Lynch, Science **298**, 1592 (2002).
- [20] C. Fuchs, Prog. Part. Nucl. Phys. **56**, 1 (2006).
- [21] A. F. Fantina, N. Chamel, J. M. Pearson, and S. Goriely, EPJ Web of Conferences **66**, 07005 (2014).
- [22] F. J. Fattoyev and J. Piekarewicz, Phys. Rev. C **86**, 015802 (2012).
- [23] J. Erler, C. J. Horowitz, W. Nazarewicz, M. Rafalski, and P.-G. Reinhard, Phys. Rev. C **87**, 044320 (2013).
- [24] M. Dutra, O. Lourenço, J. S. Sá Martins, A. Delfino, J. R. Stone, and P. D. Stevenson, Phys. Rev. C **85**, 035201 (2012).
- [25] G. A. Lalazissis, J. König, and P. Ring, Phys. Rev. C **55**, 540 (1997).
- [26] M. D. Estal, M. Centelles, X. Viñas, and S. K. Patra, Phys. Rev. C **63**, 024314 (2001).
- [27] B. G. Todd-Rutel and J. Piekarewicz, Phys. Rev. Lett. **95**, 122501 (2005).
- [28] C. J. Horowitz and J. Piekarewicz, Phys. Rev. Lett. **86**, 5647 (2001).
- [29] B. Liu, V. Greco, V. Baran, M. Colonna, and M. D. Toro, Phys. Rev. C **65**, 045201 (2002).
- [30] X. Roca-Maza, X. Viñas, M. Centelles, P. Ring, and P. Schuck, Phys. Rev. C **84**, 054309 (2011).
- [31] T. Klähn, D. Blaschke, S. Typel, E. N. E. van Dalen, A. Faessler, C. Fuchs, T. Gaitanos, H. Grigorian, A. Ho, E. E. Kolomeitsev, et al., Phys. Rev. C **74**, 035802 (2006).
- [32] R. J. Furnstahl, Nucl. Phys. **A706**, 85 (2002).
- [33] T. Sil, M. Centelles, X. Viñas, and J. Piekarewicz, Phys. Rev. C **71**, 045502 (2005).
- [34] H. Huber, F. Weber, and M. K. Weigel, Nucl. Phys. A **596**, 684 (1996).
- [35] S. Kubis and M. Kutschera, Phys. Lett. **B399**, 191 (1997).
- [36] V. Greco, M. Colonna, M. Di Toro, and F. Matera, Phys. Rev. C **67**, 015203 (2003).
- [37] R. J. Furnstahl, B. D. Serot, and H.-B. Tang, Nucl. Phys. **A598**, 539 (1996).
- [38] B. D. Serot and J. D. Walecka, Int. J. Mod. Phys. E **6**, 515 (1997).
- [39] R. J. Furnstahl, B. D. Serot, and H.-B. Tang, Nucl. Phys. **A615**, 441 (1997).
- [40] Y. Sugahara and H. Toki, Nucl. Phys. **A579**, 557 (1994).
- [41] H. Müller and B. D. Serot, Nucl. Phys. **A606**, 508 (1996).
- [42] S. K. Dhiman, R. Kumar, and B. K. Agrawal, Phys. Rev. C **76**, 045801 (2007).
- [43] B. K. Agrawal, Phys. Rev. C **81**, 034323 (2010).
- [44] M. Dutra, O. Lourenço, S. S. Avancini, B. V. Carlson, A. Delfino, D. P. Menezes, C. Providência, S. Typel, and J. R. Stone, Phys. Rev. C **90**, 055203 (2014).
- [45] A. Tamii, I. Poltoratska, P. von Neumann-Cosel, Y. Fujita, T. Adachi, C. A. Bertulani, J. Carter, M. Dozono, H. Fujita, K. Fujita, et al., Phys. Rev. Lett. **107**, 062502 (2011).
- [46] J. Piekarewicz, B. K. Agrawal, G. Colò, W. Nazarewicz, N. Paar, P.-G. Reinhard, X. Roca-Maza, and D. Vretenar, Phys. Rev. C **85**, 041302(R) (2012).
- [47] C. M. Tarbert, D. P. Watts, D. I. Glazier, P. Aguar, J. Ahrens, J. R. M. Annand, H. J. Arends, R. Beck, V. Bekrenev, B. Boillat, et al. (Crystal Ball at MAMI and A2 Collaboration), Phys. Rev. Lett. **112**, 242502 (2014).
- [48] S. Abrahamyan, Z. Ahmed, H. Albatineh, K. Aniol, D. S. Armstrong, W. Armstrong, T. Averett, B. Babineau, A. Barbieri, V. Bellini, et al., Phys. Rev. Lett. **108**, 112502 (2012).
- [49] T. W. Donnelly, J. Dubach, and I. Sick, Nucl. Phys. A **503**, 589 (1989).
- [50] W. D. Myers and W. J. Swiatecki, Nucl. Phys. **A336**, 267 (1980).
- [51] J. Carriere, C. J. Horowitz, and J. Piekarewicz, Astrophys. J. **593**, 463 (2003).
- [52] A. Sulaksono, T. J. Bürvenich, P.-G. Reinhard, and J. A. Maruhn, Phys. Rev. C **79**, 044306 (2009).
- [53] A. Sulaksono, T. Mart, T. J. Bürvenich, and J. A. Maruhn, Phys. Rev. C **76**, 041301 (2007).
- [54] J. Piekarewicz, Phys. Rev. C **76**, 064310 (2007).
- [55] S. B. Rüster, M. Hempel, and J. Schaffner-Bielich, Phys. Rev. C **73**, 035804 (2006).
- [56] S. Weinberg, *Gravitation and Cosmology* (Wiley, New York, 1972).
- [57] J. M. Lattimer, C. J. Pethick, M. Prakash, and P. Haensel, Phys. Rev. Lett. **66**, 2701 (1991).
- [58] É. É. Flanagan and T. Hinderer, Phys. Rev. D **77**, 021502(R) (2008).

- [59] T. Hinderer, *Astrophys. J.* **677**, 1216 (2008).
- [60] T. Hinderer, B. D. Lackey, R. N. Lang, and J. S. Read, *Phys. Rev. D* **81**, 123016 (2010).
- [61] F. J. Fattoyev, J. Carvajal, W. G. Newton, and B.-A. Li, *Phys. Rev. C* **87**, 015806 (2013).
- [62] T. Damour, A. Nagar, and L. Villain, *Phys Rev. D* **85**, 123007 (2012).